Electronic Supporting Information

Relaxor-to-ferroelectric crossover and disruption of polar order in 'empty' tetragonal tungsten bronzes

Jonathan Gardner[1], Fengjiao Yu[1], Chiu Tang[2], Winfried Kockelmann[3], Wuzong Zhou[1], Finlay D. Morrison[1,*]

[1]EaStCHEM School of Chemistry, University of St Andrews, North Haugh, St Andrews, KY16 9ST, UK
[2]Diamond Light Source Ltd., Harwell Science and Innovation Campus, Didcot OX11 0DE, UK
[3]ISIS Facility, Rutherford Appleton Laboratory, Chilton, Didcot OX11 0QX, UK

Structural

Variable temperature PND data for $Ba_4La_{0.67}Nb_{10}O_{30}$ (x = 0) collected on the GEM beamline at ISIS (as detailed in the main text). Rietveld refinements of data in polar space group *Bbm2* demonstrate requirement of a supercell, Figure S1.

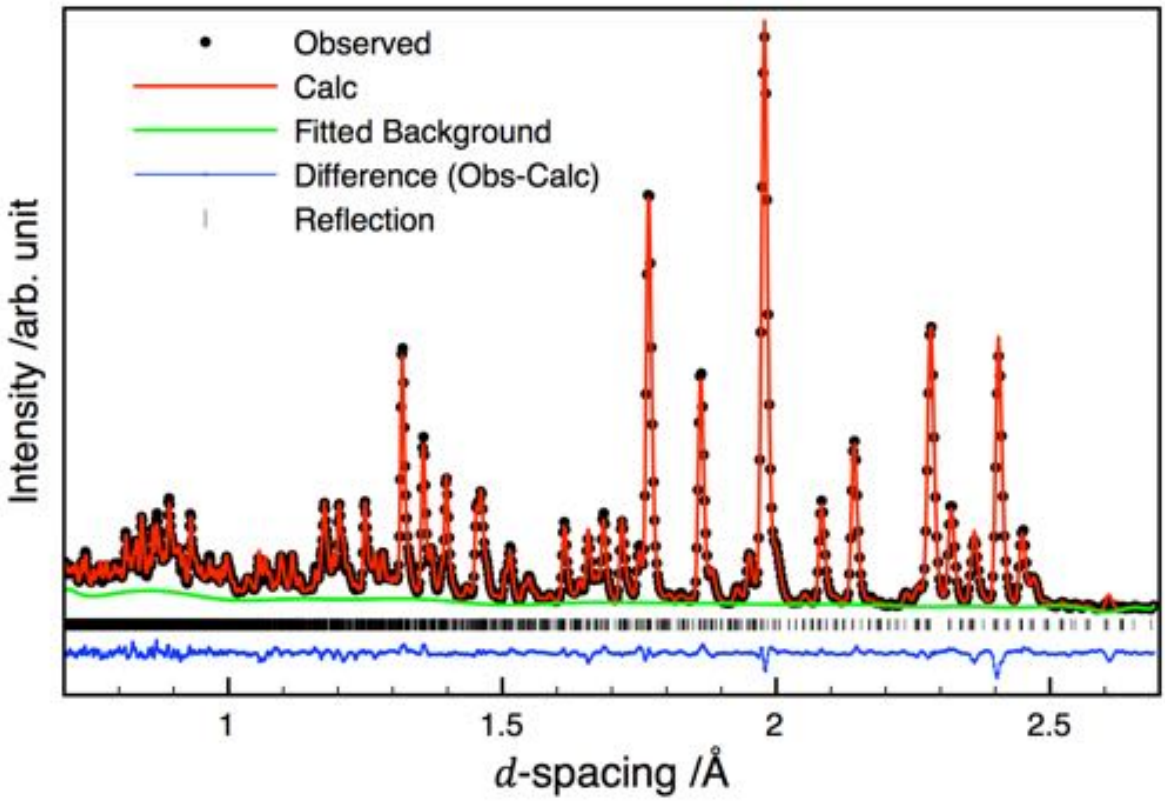

Figure S1: Rietveld refinement of PND data for $Ba_4La_{0.67}Nb_{10}O_{30}$ (x = 0) at 20 K in space group *Bbm2*; including observed data, calculated profile, fitted background, difference plot and reflection markers.

Table S1. Atomic positions of $Ba_4La_{0.67}Nb_{10}O_{30}$ (x = 0) in space group *Bbm2*

Site Label	Atom	*x*	*y*	*z*
A2_1	Ba	0.8774	0.4237	0.25
A2_2	Ba	-0.1301	0.4192	0.7484
A2_3	Ba	0.0387	0.25	0.2464
A2_4	Ba	0.0388	0.25	0.75
A2_5	Ba	0.2883	0.75	0.2485
A2_6	Ba	0.2895	0.75	0.7491
A1_1	La	0	0.5	0.2496
A1_2	La	0	0.5	0.752
A1_3	La	0.2499	0.0005	0.2456
Nb1	Nb	0.8757	0.25	0.0093
Nb2	Nb	-0.1252	0.25	0.507
Nb3	Nb	-0.1253	0.75	0.0059
Nb4	Nb	0.8753	0.75	0.5058
Nb5	Nb	0.965	0.3586	0.005
Nb6	Nb	0.9667	0.3584	0.5065
Nb7	Nb	0.2168	0.8582	0.0051
Nb8	Nb	0.2155	0.858	0.5038
Nb9	Nb	0.071	0.4334	0.0061
Nb10	Nb	0.0703	0.4307	0.5068
Nb11	Nb	0.3207	0.9322	0.0025
Nb12	Nb	0.3215	0.9319	0.5049
O1	O	0.912	0.3302	-0.0451
O2	O	0.9122	0.3338	0.505
O3	O	0.1627	0.8312	0.0055
O4	O	0.163	0.8309	0.4546
O5	O	0.9827	0.25	-0.0098
O6	O	0.9819	0.25	0.4631
O7	O	0.2333	0.75	-0.0165
O8	O	0.2333	0.75	0.5001
O9	O	0.8752	0.5334	-0.0319
O10	O	0.8754	0.535	0.5038
O11	O	0.9473	0.4641	-0.0451
O12	O	0.9438	0.4657	0.4972
O13	O	0.1968	0.964	-0.0128
O14	O	0.1965	0.9638	0.4651
O15	O	0.983	0.6046	0.0091
O16	O	0.9819	0.6092	0.448
O17	O	0.232	0.1037	0.0062
O18	O	0.2322	0.1062	0.4516
O19	O	0.916	0.6747	-0.0037
O20	O	0.9146	0.6749	0.4676
O21	O	0.1657	0.1747	-0.0348
O22	O	0.1661	0.1762	0.4881
O23	O	0.9586	0.3646	0.2329
O24	O	0.2098	0.8616	0.7343
O25	O	0.9753	0.3553	0.7329
O26	O	0.2248	0.8579	0.2334
O27	O	0.9263	0.5528	0.231
O28	O	0.1734	0.0684	0.2359
O29	O	0.9348	0.5802	0.7331
O30	O	0.1847	0.0626	0.7322
O31	O	0.8835	0.25	0.2328
O32	O	-0.1328	0.25	0.7347
O33	O	0.1298	0.25	0.2359
O34	O	0.1199	0.25	0.7356

Due to the size of the structure and presence of 55 crystallographically distinct atoms it was not possible to reliably refine atom positions and individual isotropic displacement parameters as the variables are highly correlated. Atomic coordinates listed in Table S1 are based on those obtained by Labbé and co-workers (*Journal of Physics-Condensed Matter* **1989**, 2, 25).

Table S2. Refined lattice parameters and refinement quality parameters from PND data

Temp / K	***a* / Å**	***b* / Å**	***c* / Å**	χ^2	**wR_p / %**	**$R(F^2)$ / %**
20	35.2649(30)	17.6567(15)	7.90895(19)	9.449	4.37	4.24
50	35.2656(30)	17.6573(15)	7.90899(19)	9.843	4.38	4.31
100	35.2764(30)	17.6610(14)	7.91062(18)	9.299	4.25	4.19
150	35.2851(31)	17.6644(15)	7.91206(18)	8.904	4.15	4.01
200	35.2952(31)	17.6689(15)	7.91356(18)	8.88	4.15	4.28
250	35.3085(32)	17.6741(16)	7.91528(18)	8.558	4.07	4.25
300	35.3211(34)	17.6806(16)	7.91695(19)	9.797	4.37	5.04
298	35.3223(34)	17.6814(16)	7.91664(19)	8.879	4.48	5.36
340	35.334(3)	17.6859(17)	7.91842(20)	9.404	4.62	5.74
380	35.348(4)	17.6921(19)	7.92076(21)	10.38	4.85	5.87
420	35.365(4)	17.6978(20)	7.92348(21)	10.41	4.86	6.18
450	35.378(5)	17.7022(23)	7.92545(22)	11.9	5.17	6.4
470	35.388(5)	17.7058(26)	7.92729(25)	14.09	5.63	7.08
480	35.394(6)	17.7078(28)	7.92816(26)	15.59	5.92	7.44
510	35.407(6)	17.7131(31)	7.93036(28)	18.21	6.39	7.96
550	35.424(7)	17.7206(34)	7.93310(30)	20.72	6.81	8.28
600	35.442(7)	17.730(4)	7.93619(32)	22.95	7.15	9.06

Rietveld refinement of PND data in space group *Bbm2* was carried out for all data sets collected. Refined lattice parameters at each temperature are given in Table S1. These values are that of the supercell, *c.f.* Figure 3(c) within the main text in which lattice parameters are reduced to the aristotype cell.

The quality of the refinement shows a marked deterioration at approximately 470 K (as indicated by the increase in the goodness-of-fit parameters, Figure S2) corresponding to the loss of reflections associated with the expanded TTB cell. The data points at approximately 300 K represent the change in sample environment at ambient temperature.

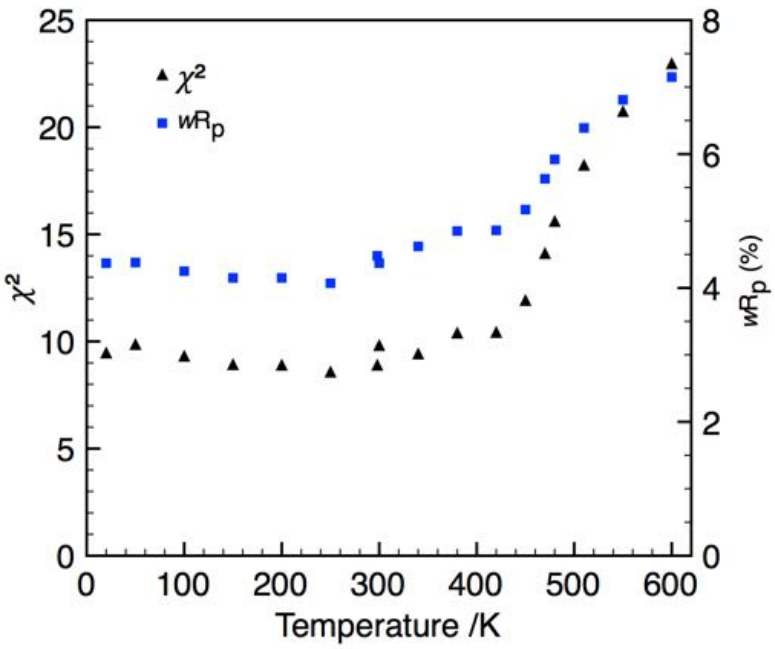

Figure S2. Refinement quality parameters; PND data for $Ba_4La_{0.67}Nb_{10}O_{30}$ (x = 0) refined using space group *Bbm2*.

As discussed above, it was not possible to refine individual isotropic displacement parameters. When values for each site type (e.g. A1-site) were constrained, Table S2, a gradual increase is observed as expected.

Table S3: Refined isotropic displacement parameters

Temp / K	μ_{iso} / Å^3			
	Ba	La	Nb	O
20	0.0081(11)	0.0038(22)	0.0048(4)	0.0050(4)
50	0.0091(12)	0.0053(23)	0.0049(4)	0.0052(4)
100	0.0088(10)	0.0074(21)	0.00571(33)	0.00549(22)
150	0.0108(11)	0.0060(22)	0.0058(4)	0.0058(4)
200	0.013(12)	0.0070(22)	0.0066(4)	0.0063(4)
250	0.0154(12)	0.0085(22)	0.0075(4)	0.0068(4)
300	0.0143(13)	0.0115(25)	0.0086(5)	0.0078(4)
298	0.0158(13)	0.0127(26)	0.0102(5)	0.0093(4)
340	0.0169(14)	0.0136(27)	0.0108(5)	0.0102(4)
380	0.0177(15)	0.0130(28)	0.0109(5)	0.0104(5)
420	0.0204(16)	0.0136(28)	0.0108(5)	0.0104(5)
450	0.0234(17)	0.0157(31)	0.0119(6)	0.0121(5)
470	0.0224(19)	0.0147(33)	0.0114(6)	0.0119(6)
480	0.0243(22)	0.014(4)	0.0112(7)	0.0126(7)
510	0.0243(22)	0.014(4)	0.0112(7)	0.0126(7)
550	0.0262(24)	0.013(4)	0.0114(8)	0.0129(7)
600	0.0283(26)	0.016(4)	0.0121(8)	0.0138(8)

Above 480 K the structure appears to have similar metrics to the basic high symmetry tetragonal aristotype (*i.e.* no reflections due to an extended superstructure are observed), however, based on synchrotron-PXRD a very slight orthorhombic distortion persists. A high temperature non-polar structure has been reported for other TTBs. The Rietveld refinement of PND data collected at 600 K with the orthorhombic non-polar space group *Pbam* is shown in figure S3. $\chi^2 = 4.471$, $wR_p = 3.19$ %

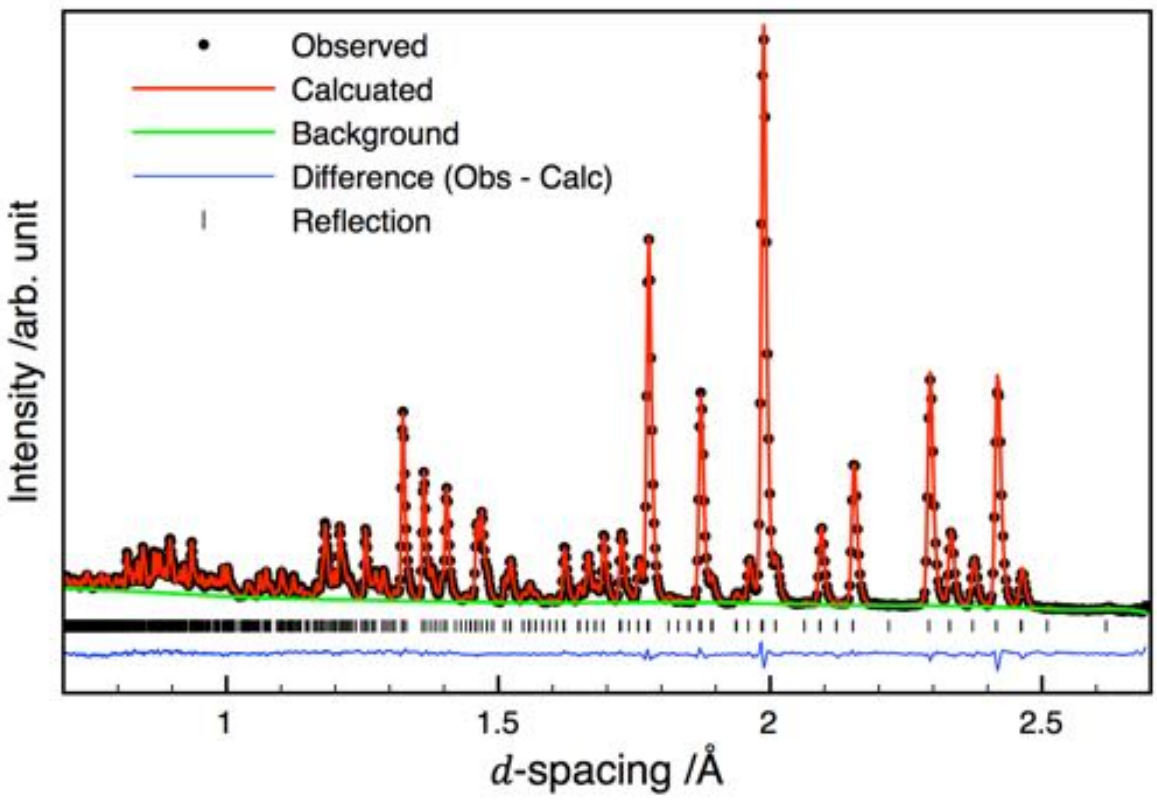

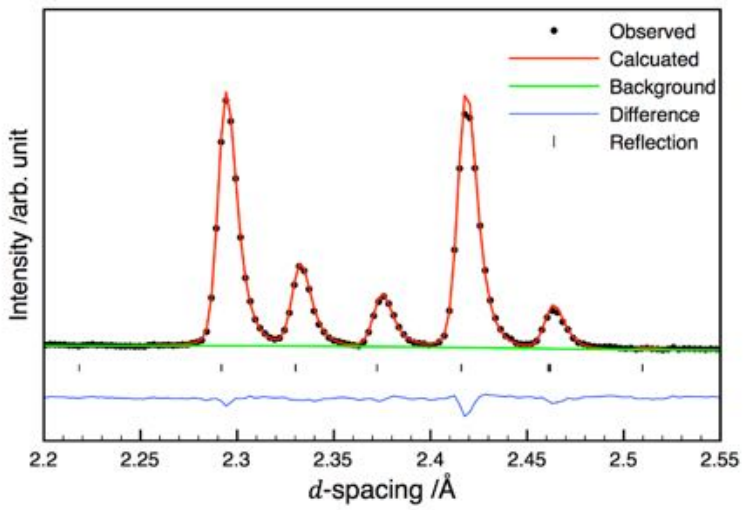

Figure S3. (a) Rietveld refinement of PND data for $Ba_4(La_{1-x}Nd_x)_{0.67}\square_{1.33}Nb_{10}O_{30}$, $x = 0$ (La) at 600 K in space group *Pbam*; (b) enlarged view of $d = 2.2$-2.55 demonstrating lack of superstructure reflections.

Synchrotron-PXRD data was collected on cooling from 500 K to 100 K for $Ba_4La_{0.67}Nb_{10}O_{30}$ (x = 0) on beamline I11 at the Diamond Light Source. A Rietveld refinement of data collected at 100 K using the same *Bbm2* structural model is shown in Figure S4 (χ^2 = 6.258, wR_p = 11.13 %). Figure S5 depicts enlarged sections of the same refinement. As with neutron data, individual atom positions and μ_{iso} were not refined.

The deficiencies in the refinement are principally from peak shape and intensity. Refinement of the positions of atoms in the A2 site (Ba^{2+}) and no others (data not shown) led to improvements of the fit (χ^2 = 5.690, wR_p = 9.58 %) indicating that while atom positions may be similar to the model described in the main text and which is based on the $Ba_4Na_2Nb_{10}O_{30}$ structural model of Labbé (Ref 25 in the main text), it is not identical.

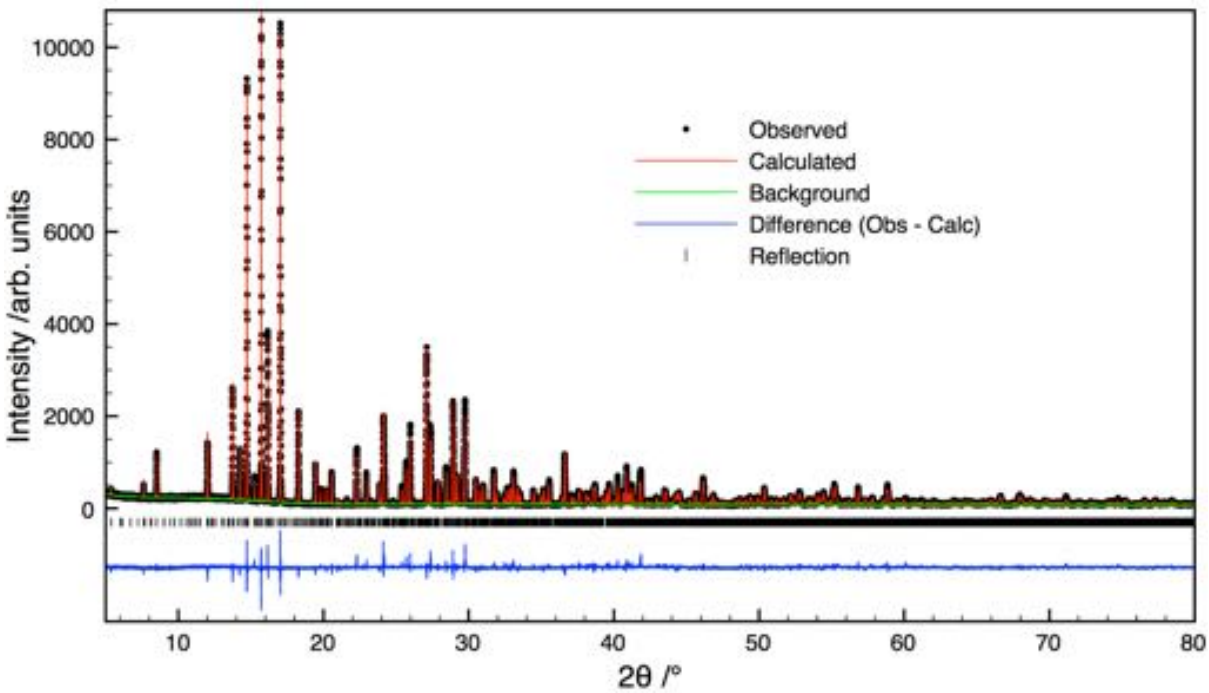

Figure S4. Rietveld refinement of s-PXRD data for $Ba_4(La_{1-x}Nd_x)_{0.67}\square_{1.33}Nb_{10}O_{30}$, x = 0 (La) at 100 K in space group *Bbm2*.

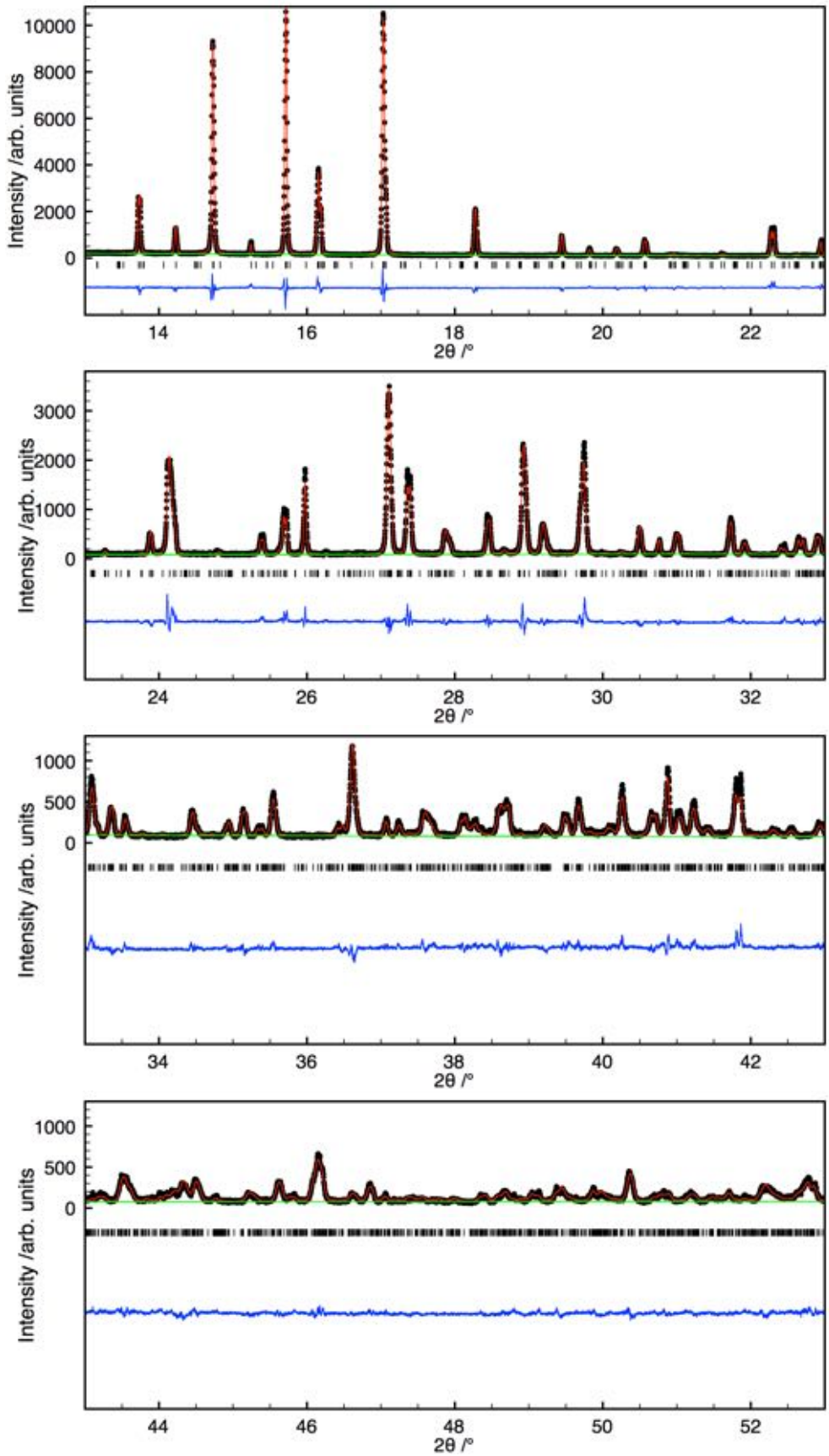

Figure S5. Enlarged sections of Figure S4 – s-PXRD data for $Ba_4(La_{1-x}Nd_x)_{0.67}\square_{1.33}Nb_{10}O_{30}$; $x = 0$ (La) at 100 K in space group *Bbm2*.

Thermal expansion

Synchrotron PXRD data of $Ba_4La_{0.67}Nb_{10}O_{30}$ (x = 0) indicates two regimes of linear thermal expansion at low and high temperature, Figure 3(c). The thermal expansion coefficient, α, for individual cell parameters was calculated. Values obtained are as expected for an oxide material. Thermal expansion rate is greater in the higher temperature region (above 270 K) and is larger in *a*.

Table S4. Thermal expansion coefficients for $Ba_4La_{0.67}Nb_{10}O_{30}$ (x = 0) as determined form s-PXRD data.

Axis direction	Linear thermal expansion coefficients, α_L (10^{-6} K^{-1})	
	Low T (< 270 K)	High T (> 270 K)
a	6.78	11.3
b	5.49	7.64
c	2.56	7.47

Dielectric properties

Dielectric data for the intermediate compositions, Figure S6, demonstrates the decreasingly diffuse nature of the low temperature peak with increasing *x* (decreasing A1-cation size). The data correlate with the observed *P-E* behaviour (Figures S8-10) which indicate a crossover from relaxor ferroelectric (RFE) to more 'normal' ferroelectric-like behaviour as the two peaks coalescence.

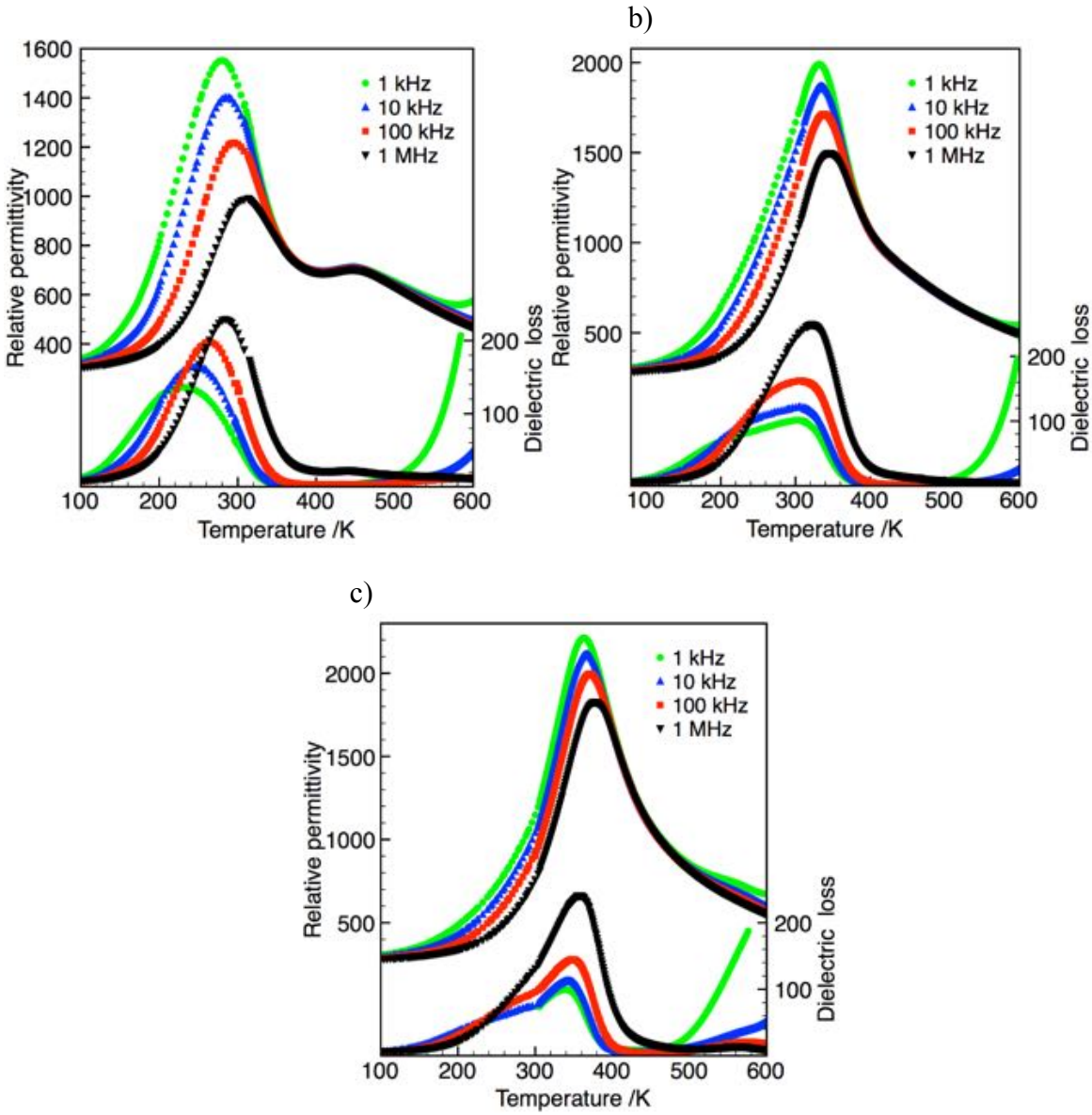

Figure S6. Relative permittivity (ε') and dielectric loss (ε") for $Ba_4(La_{1-x}Nd_x)_{0.67}Nb_{10}O_{30}$ at selected frequencies for: (a) $x = 0.25$, (b) $x = 0.5$ and (c) $x = 0.75$

With increasing *x*, the contribution of the high temperature relaxation is shown to become more influential, Figure S7.

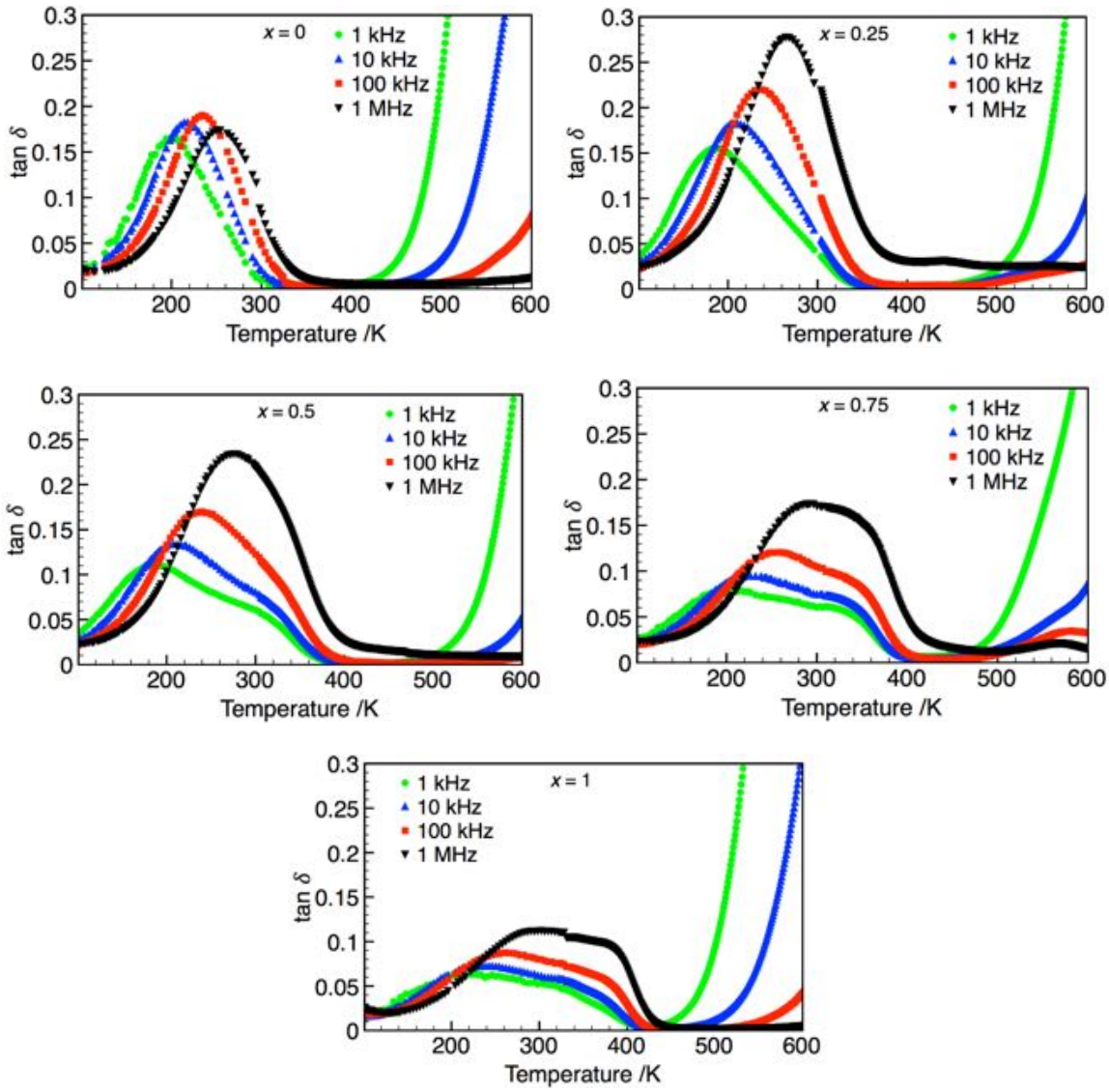

Figure S7. Dielectric loss, tan δ, for $Ba_4(La_{1-x}Nd_x)_{0.67}Nb_{10}O_{30}$ at selected frequencies for *x* = 0, 0.25, 0.5, 0.75, 1.

Polarisation–Field (P-E) measurements for $Ba_4(La_{1-x}Nd_x)_{0.67}Nb_{10}O_{30}$

Polarisation *vs.* field measurements for $x = 0$ (Figure S8), $x = 0.25$ (Figure S9), $x = 0.5$ (Figure S10) and $x = 0.75$ (Figure S11). All compounds are ferroelectric at low temperature; well-saturated ferroelectric hysteresis loops are observed which become slimmer with increasing temperature. As with $Ba_4La_{0.67}Nb_{10}O_{30}$ ($x = 0$) P-E loops with 'pinched' character are recorded in the temperature range between the two peaks in the dielectric data shown for $x = 0.25$. No indication of the onset of such pinched loops is observed for $x = 0.75$ or $x = 1$; for these compositions the saturated P-E loop becomes slimmer and at high temperature a linear dielectric response indicates loss of ferroelectricity.

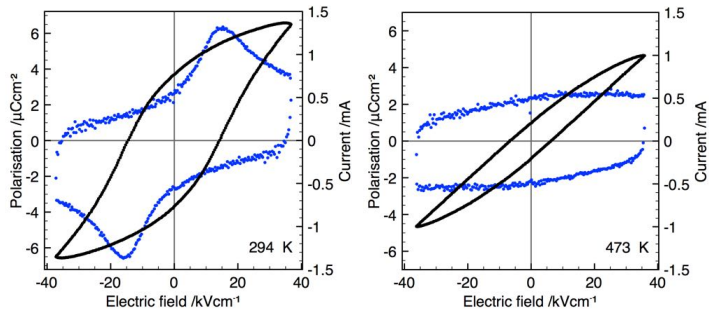

Figure S8. P-E data for $Ba_4(La_{1-x}Nd_x)_{0.67}Nb_{10}O_{30}$, $x = 1$, obtained at 100 Hz.

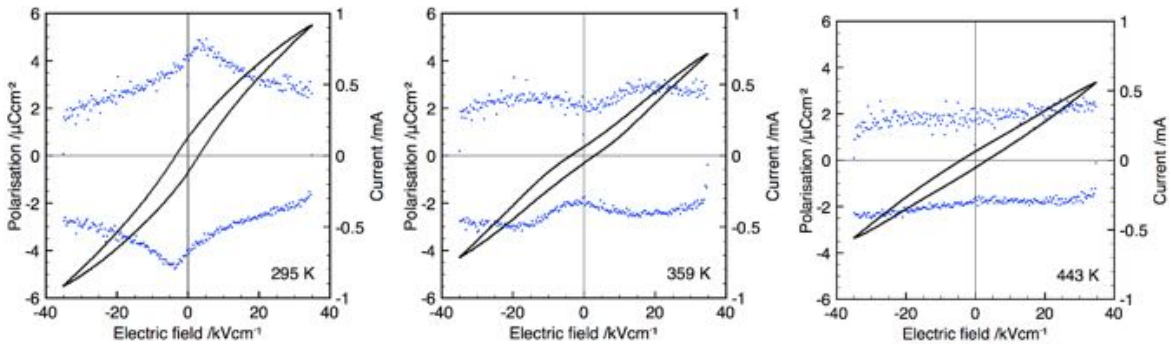

Figure S9. Variable temperature P-E data for $Ba_4(La_{1-x}Nd_x)_{0.67}Nb_{10}O_{30}$, $x = 0.25$ (100 Hz).

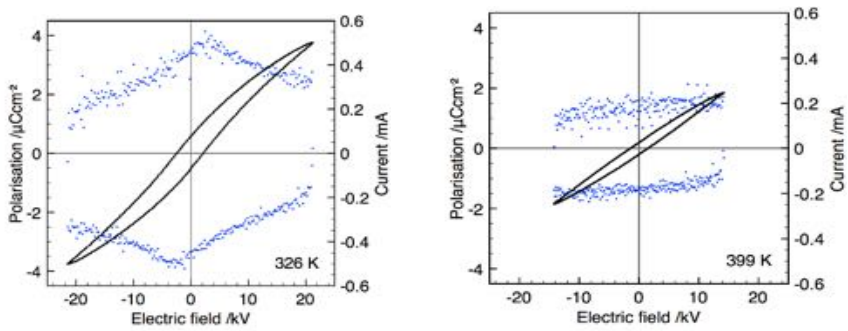

Figure S10. P-E data for $x = 0.5$ (100 Hz)

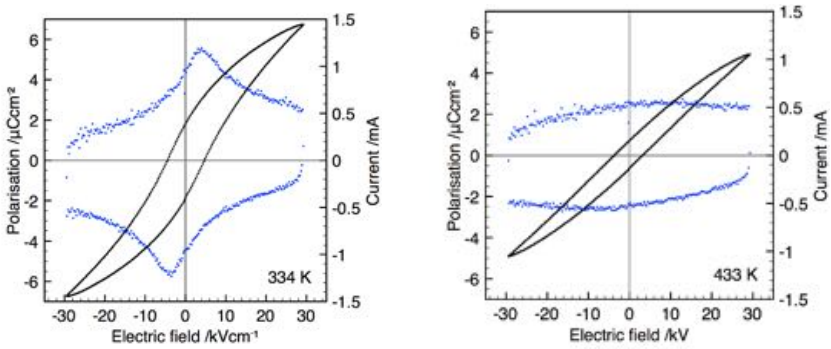

Figure S11. P-E data for x = 0.75 (100 Hz)

Quenching

Samples of $Ba_4La_{0.67}Nb_{10}O_{30}$ (x = 0) were air quenched from high temperature.

Samples with sputtered Au electrodes were heated to 623 K (350 °C) for 2 hours and short circuited while earthed. Samples were then air quenched and data collected immediately. 'Pinched' behaviour persists, Figure S12.

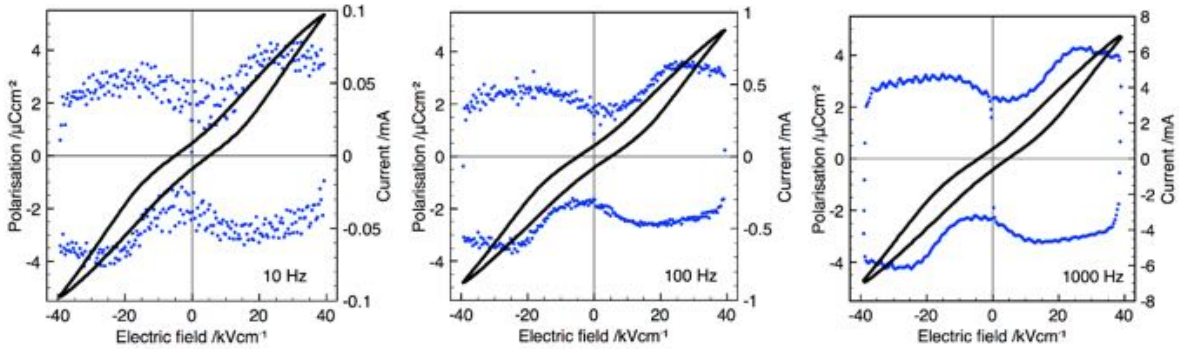

Figure S12. P-E data for sample quenched from 623 K at 10 Hz, 100 Hz and 1000 Hz demonstrating retention of pinched character of P-E loop, (295 K).

Higher temperature quenching experiments were also carried out; samples were heated to 1273 K (1000 °C) for 2 hours and air quenched. Sputtered electrodes may degrade at such temperatures so silver conductive paint was applied as soon as samples were cool enough and data recorded (within 30 minutes of quenching). Again 'pinched' behaviour persists, Figure S13.

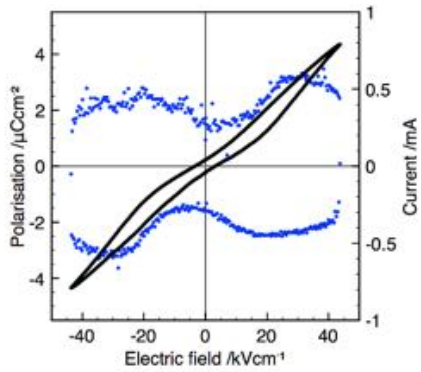

Figure S13. P-E data for sample quenched from 1273 K demonstrating retention of the pinched character of P-E loop, 100 Hz, ambient temperature (295 K).

Fatigue measurements

A sample of $Ba_4La_{0.67}Nb_{10}O_{30}$ (x = 0) was fatigued for 1×10^7 cycles with an applied electric field of 40 $kVcm^{-1}$ (fatigue frequency = 10 kHz) at ambient temperature (296 K). P-E data (applied field 40 $kVcm^{-1}$, 100 Hz) was recorded at specific points during the fatiguing process. There is little appreciable difference between the first and last loop, Figure S14.

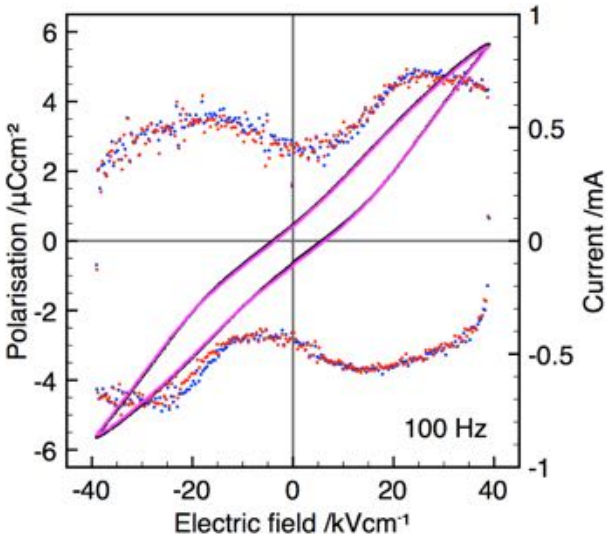

Figure S14. Comparison of 1st (polarisation data in black, current data in blue) and last (1×10^7) cycle (polarisation data purple, current data red), recorded at ambient temperature.

The maximum polarisation (P_{max}) and the remenant polarisation (P_r) do not significantly change during the fatiguing process, Figure S15

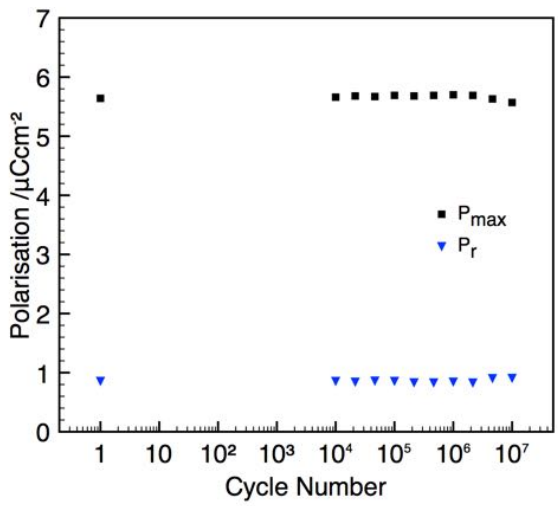

Figure S15. Maximum polarisation and remenant polarisation during fatiguing process.